Available online at www.sciencedirect.com
ScienceDirect
Applied Thermal Engineering 27 (2007) 1182–1190
Applied Thermal Engineering
www.elsevier.com/locate/apthermeng

Dynamic modelling and optimisation of cryogenic systems

M. Rodríguez, M.S. Diaz *

Planta Piloto de Ingeniería Química, PLAPIQUI (UNS-CONICET), Camino La Carrindanga Km 7, 8000 Bahia Blanca, Argentina

Received 20 December 2005; accepted 8 February 2006
Available online 5 May 2006

Abstract

This work addresses the dynamic optimisation of the cryogenic sector in a large-scale natural gas processing plant. Main attention is focused on rigorous dynamic modelling of countercurrent heat exchangers with phase change and a subsequent high-pressure separation tank. The original distributed parameter problem, which results from dynamic energy balances in countercurrent heat exchangers, is transformed into an ordinary differential system (ODE) by performing spatial discretisation with the method of lines. The entire model comprises algebraic equations for thermodynamic predictions with the Soave–Redlich–Kwong (SRK) equation of state, hydraulic and design equations. The differential-algebraic equation (DAE) optimisation problem is solved with an advanced simultaneous strategy that transforms the original problem into a large-scale nonlinear programming (NLP) problem through discretisation in time of the entire set of variables by collocation on finite elements. Model resolution provides optimal temporal and spatial profiles for pressure and temperature in heat exchangers, together with partial condensation description.

Keywords: Dynamic optimisation; Cryogenic heat exchanger; Partial condensation; Large-scale NLP

1. Introduction

Dynamic modelling and optimisation of chemical processes are currently accepted due to the broad range of benefits that can be derived from their application. However, the complex and large-scale nature of these problems has prevented their solution in real plant cases until the development of appropriate resolution techniques. Cervantes and Biegler [3] proposed an advanced simultaneous strategy for dynamic optimisation of large-scale problems. More recently, Diaz et al. [8] analysed optimal switching between operating modes in cryogenic distillation columns through the formulation of rigorous dynamic optimisation models including predictions of carbon dioxide precipitation conditions at each stage in the column. Raghunathan et al. [10] extended the model to account for phase verification through the inclusion of MPECs (mathematical programs with equilibrium constraints).

The transient responses of countercurrent heat exchangers have been represented by empirical equations by Romie [11]. Lakshmanan and Potter [9] developed a mathematical model determining analytical solutions to simulate the dynamic behaviour of countercurrent heat exchangers. They proposed a numerical scheme to obtain accurate solution of the dynamic models based on convective transport occurring in various countercurrent operations. Yin and Jensen [13] investigated the temperature transient response in a heat exchanger using an integral method to approximate the dynamic behaviour of the heat exchanger, which has one fluid with constant temperature and the other fluid remains single phase. Correa and Marchetti [5] developed a multicell dynamic simulation model to describe the transient behaviour of a multipass shell-and-tube heat exchanger with baffles. They proposed dividing the heat exchanger into a number of lumped elements where a small part of the heat transfer operation takes place. The resulting model was appropriate for simulating a number of start-up alternatives and obtaining the dynamic responses to flowrate or temperature disturbances.

* Corresponding author.
E-mail address: sdiaz@plapiqui.edu.ar (M.S. Diaz).

1359-4311/$ - see front matter © 2006 Elsevier Ltd. All rights reserved.
doi:10.1016/j.applthermaleng.2006.02.044

Nomenclature

A_{sup}	superficial area per length (m^2/m)
A_t	heat transfer area in tubes (m^2)
C_p	heat capacity of fluid (kJ/kmole K)
C_v	valve flow capacity ($gpm/Psi^{0.5}$)
D_{in}	diameter of tube (inside) (m)
F_j	fluid flowrate (kg/min)
G	mass velocity inside tube (kg/min)
h	liquid enthalpy (MJ/kmole)
H	vapour enthalpy (MJ/kmole)
h_p	liquid enthalpy in previous step (MJ/kmole)
H_p	vapour enthalpy in previous step (MJ/kmole)
h_t	liquid height in the tank (m)
K_{ij}	equilibrium ratio for component j in grid point i
K_f	Bell-Delaware correlation
L	liquid flowrate (kmole/min)
Long	length of straight tube (m)
L_p	liquid flowrate in previous step (kmole/min)
M	total holdup (kmole)
M_L	liquid holdup (kmole)
m_{VL}	interfacial mole flowrate (kmole/min)
M_V	vapour holdup (kmole)
M_W	molecular weight
P_{mol_L}	liquid molecular weight
P_{mol_t}	molecular weight in tubes
P_{mol_V}	vapour molecular weight
P_s	pressure in shell (bar)
P_{sp}	pressure in shell in previous step (bar)
P_t	pressure in tubes (bar)
Q_t	net rate of heat transfer in tubes (MJ/min)
r	high-pressure separation tank radio (m)
Re	Reynolds number
R	gas constant (m^3 bar/K kmole)
R_L	pressure drop correction factor for baffle leakage effects
t	time (min)
T_s	fluid temperature in shell (K)
T_t	fluid temperature in tubes (K)
V	vapour flow rate (kmole/min)
V_{max}	maximum velocity (m/s)
Vol_V	vapour volume (m^3)
V_p	vapour flow rate in previous step (kmole/min)
v_t	fluid velocity in tubes (m/min)
x	liquid mole fraction
y	vapour mole fraction
z	compressibility factor

Subscripts

i	cell
j	component

Greek symbols

ρ_L	liquid density (kg/m^3)
ρ_r	density at reference temperature (kg/m^3)
ρ_t	fluid density in tubes (kg/m^3)
ρ_V	vapour density (kg/m^3)
ϕ_L	liquid fugacity coefficient
ϕ_V	vapour fugacity coefficient
μ	viscosity of fluid (Pa s)
ΔP_c	pressure drop at cross-flow zone (bar)
ΔP_s	pressure drop (bar)
ΔP_w	pressure drop at window zone (bar)
Δz	length of each cell (m)

Regarding the simulation of heat exchangers with phase change, Zinemanas et al. [14] proposed an algorithm for the simulation of horizontal or vertical 1–1 shell and tubes heat exchangers with phase change and one or more components. The algorithm calculated local values of the variables along the heat exchangers and accommodates changes of flow patterns. They based the calculation on a numerical integration with constant enthalpy steps. For each step the physical properties (temperature, phase composition and pressure drop) were a function of the operating conditions for that step.

As heat exchangers are part of larger industrial processes and systems, transient operation can occur frequently, and the transient response of the heat exchanger can affect overall system performance. They are exposed to transient behaviour not only during start up and shut down operations, but also due to variations of external loads that lead to disturbances in inlet temperature and flowrate of fluid streams and changes of heat transfer conditions. Knowledge of transient response of shell and tube heat exchangers is required for process control and optimal operation. However, dynamic optimisation modelling for heat exchangers with phase change has hardly been addressed due to its complex and large-scale nature.

In this work, we have performed dynamic modelling and optimisation of main units in the cryogenic sector of natural gas turboexpansion plants, which include countercurrent heat exchangers with phase change and high-pressure separation tanks. The model comprises differential energy and mass balances, hydraulic correlations and rigorous thermodynamic predictions with the Soave–Redlich–Kwong SRK, [12] equation of state for equilibrium calculations. Energy balances for countercurrent heat exchangers give rise to a distributed parameters problem that is in turn transformed into an ordinary differential one, through spatial discretisation applying the method of lines. The dynamic optimisation problem, which includes both ordinary differential equations and algebraic ones as constraints (DAE), has been solved through a simultaneous strategy [2]. This approach proceeds by

discretising the DAE system by collocation on finite elements. The resulting large-scale nonlinear programming (NLP) problem is solved with a reduced space successive quadratic programming algorithm [4]. The solution of the DAE optimisation problem provides state and control variables profiles in space and time, as well as a detailed description of partial phase change in countercurrent heat exchangers.

2. Process description

In typical turboexpansion plants that extract ethane from natural gas, the feed gas is cooled both in countercurrent cryogenic heat exchangers with residual gas and in demethanizer side and bottom reboilers. The partially condensed gas feed is sent to a high-pressure separator. The vapour is expanded through a turboexpander to obtain the low temperatures required for high ethane recovery and is fed to a demethanizer column. The liquid from the high-pressure separator enters the demethanizer at its lowest feed point. Methane and nitrogen constitute top product and ethane and heavier hydrocarbons are obtained as bottom product. Carbon dioxide is distributed between top and bottom streams.

In this work, special attention has been devoted to dynamic modelling of the system consisting of shell and tube cryogenic heat exchangers and high-pressure separators. In particular, rigorous dynamic models for cryogenic heat exchangers, where natural gas phase change (partial condensation) takes place, have required special effort and these models are described in the following section.

3. Optimisation strategy

The general formulation of the differential algebraic equation (DAE) optimisation problem is as follows:

$$
\begin{aligned}
\min \quad & \Phi(z(t_f), y(t_f), u(t_f), t_f, p) \\
\text{s.t.} \quad & \frac{dz(t)}{dt} = f(z(t), y(t), u(t), p, t) \\
& h(z(t), y(t), u(t), p, t) = 0 \\
& z(0) = z_0 \\
& h_S(z(t_S), y(t_S), u(t_S), p, t_S) = 0 \\
& z(t) \in [z_l, z_u], \quad y(t) \in [x_l, x_u] \\
& u(t) \in [u_l, u_u], \quad p \in [p_l, p_u] \\
& t_t \in [t_{fl}, t_{fu}]
\end{aligned}
$$

where Φ is a scalar objective function; f is the right hand side of differential equations constraints; h are algebraic equation constraints, h_S are additional point conditions at times t_S; z are differential state variables; z_0 are the initial values of z; y are algebraic state variables; u are control variables; p are time independent variables and t_f is the final time. This system presents initial condition and point conditions at time t_S.

The dynamic optimisation model for the cryogenic system has been formulated within a simultaneous optimisation approach [4] in which profiles for both state and optimisation variables are represented as piecewise polynomials over finite elements in time and the DAE system is discretised by orthogonal collocation over these finite elements. In this way, the DAE optimisation problem is transformed into a large-scale nonlinear programming (NLP) one that requires special solution strategies. In particular, we have applied a barrier point method with successive quadratic programming (SQP) techniques, within program IPOPT [4]. The main idea in the barrier method is to solve successive parametric NLPs, for decreasing values of the barrier parameter, each of them giving a solution that is used as a good initial point for the following barrier problem. Besides, each parametric NLP is an equality constrained problem and can be solved by the application of reduced Hessian SQP techniques, with the advantage of presenting unconstrained quadratic subproblems, of straightforward resolution [2].

4. Mathematical model

Cryogenic heat exchangers are baffled shell-and-tube single-pass countercurrent ones, in which the fluid in the tubes is residual gas (mainly methane), and the fluid in the shell is natural gas. The partially condensed natural gas coming out of cryogenic heat exchangers is sent to a high-pressure separation tank. Fig. 1 shows the diagram of the system with heat exchangers and high-pressure separator and Table 1 shows both fluids composition. A detailed description of the models is given below.

4.1. Cryogenic heat exchangers

In these heat exchangers, inlet natural gas is cooled and partially condensed in countercurrent flow with residual

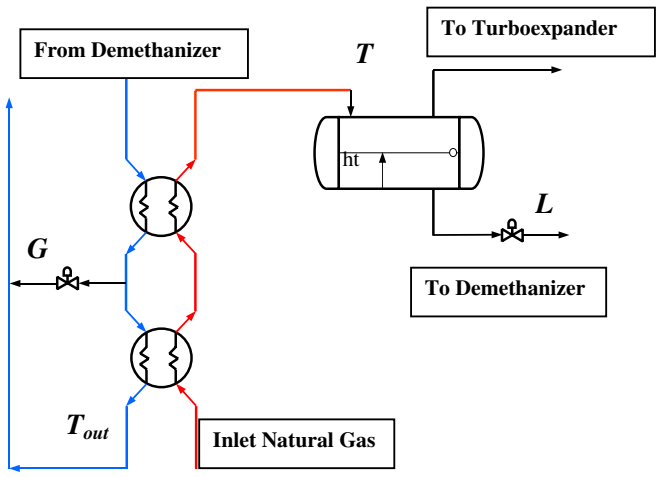

Fig. 1. Cryogenic heat exchangers and high-pressure separator system.

Table 1
Natural gas and residual gas compositions

Component	Natural gas	Residual gas
N_2	0.0144	0.01554
CO_2	0.0065	0.00440
CH_4	0.9043	0.96746
C_2H_6	0.0461	0.01175
C_3H_8	0.0176	0.00031
C_4H_{10}	0.0033	7.70E−06
C_4H_{10} (iso)	0.0044	3.34E−06
C_5H_{12}	0.0015	9.32E−08
C_5H_{12} (iso)	0.0009	1.68E−08
C_6H_{14}	0.0010	1.36E−09

gas coming from the top of the demethanizer column. There are two consecutive heat exchangers and partial condensation of natural gas takes place within the second one. Fluid temperatures vary not only along the heat exchanger but also with time at each point. This process is modelled by a partial differential equations (PDE) system. In this work, the PDE system is transformed into an ordinary differential equations (ODE) system by the application of the method of lines for the discretisation along the heat exchanger, which gives rise to the model shown in Fig. 2, which is also referred to as the multicell model.

4.1.1. Heat exchanger with single phase flow

To model the cryogenic heat exchanger with single phase flow, the main assumptions are that the inside surface of the shell is adiabatic, heat transfer area is uniformly distributed, heat transfer coefficients are constant, longitudinal heat conduction within fluids is neglected, cross sectional area is constant, thermal resistance of the wall to heat transfer is neglected. Dynamics of tube walls are assumed small enough to be negligible, thus any accumulation of energy within the elemental ring is entirely due to the fluids occupying the elements. However, if the wall dynamics had to be taken into account, only an additional energy balance should be required for the tube walls.

We have performed energy balances on microscopic elements on both shell and tube sides, considering the amount of energy entering and leaving the element with the flowing fluid and the amount of energy coming in through the tube wall over the time interval. These balances give rise to the following first order hyperbolic partial differential equation (PDE) system:

Tube side

$$\frac{\partial T_t(z,t)}{\partial t} + v_t \frac{\partial T_t(z,t)}{\partial z} = \frac{h_t * A_{sup}}{\rho_t * C_{p_t} * A_t * L}(T_s(z,t) - T_t(z,t)) \quad (1)$$

Shell side

$$\frac{\partial T_s(z,t)}{\partial t} - v_s \frac{\partial T_s(z,t)}{\partial z} = \frac{h_s * A_{sup}}{\rho_s * C_{p_s} * A_s * L}(T_t(z,t) - T_s(z,t)) \quad (2)$$

with the following initial (a starting temperature profile) and boundary conditions (inlet fluid conditions, at $z = 0$ and $z = L$, respectively) for both sides:

$$T_t(0,t) = T_t \circ (t)$$
$$T_s(L,t) = T_s \circ (t)$$
$$T_t(z,0) = T_t * (z)$$
$$T_s(z,0) = T_s * (z)$$

The second term in the left hand side in Eqs. (1) and (2) involves fluid velocity either in the tubes (v_t) or in the shell (v_s) and a temperature gradient in the spatial coordinate z. It is known as the convective term, indicating the rate of heat transfer due to fluid motion or convection.

We have applied the method of lines to spatially discretise this PDE system into sets of ordinary differential equations (ODE). Backward finite differences have been applied to the convective term, as it has been proved that they provide good approximations for this type of term. In this way, each partial differential equation gives rise to the following set of ordinary differential equations for each grid point:

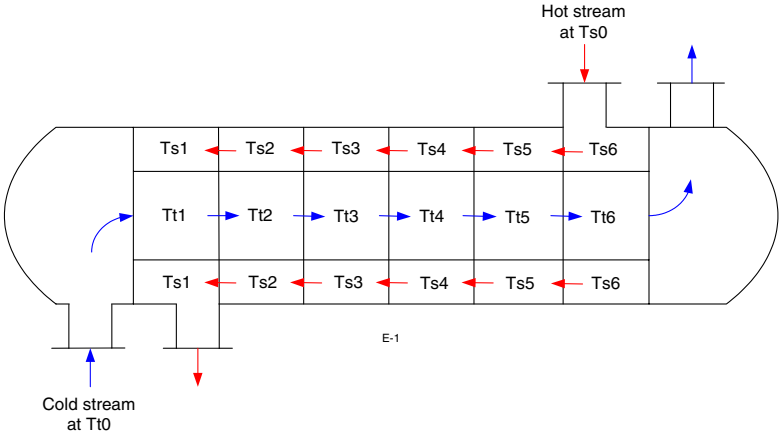

Fig. 2. Multicell model.

Tube side

$$\frac{dT_{t_i}}{dt} = -\frac{v_{t_i}}{\Delta z}(T_{t_i} - T_{t_{i-1}}) + \frac{h_t * A_{sup}}{\rho_{t_i} * C_{p_t} * A_t * L}(T_{s_i} - T_{t_i}) \quad (3)$$

Shell side

$$\frac{dT_{s_i}}{dt} = \frac{v_{s_i}}{\Delta z}(T_{s_i} - T_{s_{i-1}}) + \frac{h_s * A_{sup}}{\rho_{s_i} * C_{p_s} * A_s * L}(T_{t_i} - T_{s_i}) \quad (4)$$

The model includes algebraic equations that incorporate the functionality of the density, the compressibility factor and the velocity with temperature at each grid point i

$$\rho_{j,i} = \frac{M_W * P}{z_{j,i} * R * T_{j,i}} \quad (5)$$

$$v_{j,i} = \frac{F_j}{\rho_{j,i} * A_j} \quad (6)$$

$$z_{j,i} = a_j + b_j * T_{j,i} \quad (7)$$

where j refers either to shell or tube side, and a_j and b_j are constants that have been determined through rigorous steady state process simulations [6,7] based on SRK equation of state [12] predictions.

4.1.2. Heat exchanger with phase change

The model of an exchanger with phase change consists of two parts: the submodel of the two-phase flow and the submodel of the single phase flow. For tube side fluid (residual gas), a single phase flow is considered, represented by sets of equations (3), (5), (6) and (7). For shell side fluid (natural gas), partial condensation takes place and a two-phase flow model has been formulated. Basic assumptions are that vapour and liquid are in thermodynamic equilibrium, but they may have different velocities; the flow is one-dimensional, i.e., the vapour and the liquid each have an average cross-sectional velocity and the void fraction is used to describe the ratio of cross-sectional area occupied by the vapour to the total cross-sectional area. Mass balances for both the liquid and vapour phase have been formulated, where $m_{VL,i}$ is the interfacial mole transport rate from vapour to liquid phase. Having performed the spatial discretisation, the following equations constitute the model:

Vapour phase

$$\frac{dM_{V,i}}{dt} = V_{i-1} - V_i - m_{VL,i} \quad (8)$$

Liquid phase

$$\frac{dM_{L,i}}{dt} = L_{i-1} - L_i + m_{VL,i} \quad (9)$$

Since thermodynamic equilibrium between phases is assumed at any instant, only one energy balance for the mixture is required, where E refers to internal energy

$$\frac{dE_i}{dt} = L_{i-1} * h_{i-1} + V_{i-1} * H_{i-1} - L_i * h_i - V_i * H_i + Q_i^t \quad (10)$$

Pressure profile along the heat exchanger has been calculated at each grid point assuming steady state conditions through the Bell-Delaware method [1], which takes into account exchanger geometry, fluid type and velocity. The exchanger configuration and design parameters are reported in Table 2. Algebraic equations for pressure drop include:

$$P_{sp_i} - P_{s_i} = \Delta P_{s_i} \quad (11)$$

$$\Delta P_{s_i} = (A * \Delta P_{c_i} + B * \Delta P_{w_i}) * R_L + C * \Delta P_{c_i} \quad (12)$$

$$\Delta P_{c_i} = (K_a + N_c * K_{f_i}) * \left(\frac{\rho_{V_i} * V_{max_i}^2}{2}\right) \quad (13)$$

$$\Delta P_{w_i} = \frac{(2 + 0.6 * N_{cw}) * \dot{m}t_i^2}{\rho_{V_i}} \quad (14)$$

$$K_{f_i} = A + \frac{B}{Re_i} - \frac{C}{Re_i^2} + \frac{D}{Re_i^3} - \frac{E}{Re_i^4} \quad (15)$$

$$Re_i = \frac{\rho_{V_i} * V_{max_i} * D_{in}}{\mu} \quad (16)$$

with A, B, C, D, E corresponding to Bell-Delaware method and K_a, N_c and N_{cw} are calculated as function of heat exchanger geometry.

Algebraic equations also include rigorous thermodynamic predictions. The main algebraic equations for each grid point i are

Internal energy:

$$E_i = M_{V,i}H_i + M_{L,i}h_i \quad (17)$$

Equilibrium ratio for component j ($K_{i,j}$):

$$K_{i,j} = \frac{\phi_{i,j}^L}{\phi_{i,j}^V} \quad (18)$$

$$y_{i,j} = K_{i,j}x_{i,j} \quad (19)$$

Summation equations:

$$\sum_j y_{i,j} - \sum_j x_{i,j} = 0 \quad (20)$$

Vapour (H_i) and liquid enthalpy (h_i) calculation:

Table 2
Heat exchanger configurations and design parameters

Shell internal diameter (m)	0.928
Tube outside diameter, D_0 (m)	0.019
Tube pitch, P_T (m)	0.0254
Array	△ (triangular)
Number of tubes, N_T	990
Number of tube pass, N_{T_p}	1
Number of shell pass, N_{T_s}	1
Baffle spacing, L_B (m)	0.6096
Shell length, L_s (m)	12.192
Bundle-to-shell diametral clearance, Δ_b (m)	0.0695
Thickness of baffle, t_b (m)	0.005
Baffle cut (%)	40

$$H_i = H_i^{\text{ideal}} - \Delta H_i \tag{21}$$

$$H_i^{\text{ideal}} = \sum_{j=1}^{n_c} H_{i,j}^{\text{ideal}}(T_i) y_{i,j} \tag{22}$$

$$h_i = h_i^{\text{ideal}} - \Delta h_i \tag{23}$$

$$h_i^{\text{ideal}} = \sum_{j=1}^{n_c} h_{i,j}^{\text{ideal}}(T_i) x_{i,j} \tag{24}$$

where ΔH_i and Δh_i correspond to residual enthalpies. These functions, together with fugacity coefficients and compressibility factors for both liquid and vapour phases are calculated with SRK equation of state [12]:

Residual enthalpies:

$$\Delta H_i = \Delta H(T_{s_i}, P_{s_i}, y_{i,j}) \tag{25}$$

$$\Delta h_i = \Delta h(T_{s_i}, P_{s_i}, x_{i,j}) \tag{26}$$

Compressibility factor:

$$z_i^{\text{V}} = z^{\text{V}}(T_{s_i}, P_{s_i}, y_{i,j}) \tag{27}$$

$$z_i^{\text{L}} = z^{\text{L}}(T_{s_i}, P_{s_i}, x_{i,j}) \tag{28}$$

Fugacity coefficients:

$$\phi_{i,j}^{\text{V}} = \phi^{\text{V}}(T_{s_i}, P_{s_i}, y_{i,j}) \tag{29}$$

$$\phi_{i,j}^{\text{L}} = \phi^{\text{L}}(T_{s_i}, P_{s_i}, x_{i,j}) \tag{30}$$

The corresponding equations are presented in Appendix A.

Vapour ($\rho_{\text{V},i}$) and liquid density ($\rho_{\text{L},i}$):

$$\rho_{\text{V},i} = \frac{P_{s_i} * P^{\text{V}}_{\text{mol}_{s_i}}}{z_i^{\text{V}} * R * T_{s_i}} \tag{31}$$

$$\rho_{\text{L},i} = \frac{P_{s_i} * P^{\text{L}}_{\text{mol}_{s_i}}}{z_i^{\text{L}} * R * T_{s_i}} \tag{32}$$

4.2. High-pressure separator

The partially condensed mixture from the cryogenic heat exchangers enters a high-pressure horizontal tank where vapour and liquid streams are separated. The model includes an overall dynamic mass balance and geometric equations relating liquid content in the tank to liquid height and liquid flowrate as function of pressure drop over the valve.

Overall mass balance:

$$\frac{\text{d}M}{\text{d}t} = L_{\text{p}} + V_{\text{p}} - L - V \tag{33}$$

Vapour volume (Vol_{V}):

$$\text{Vol}_{\text{V}} = \pi r^2 \text{Long} - \frac{M_{\text{L}}}{\rho_{\text{L}}/P_{\text{mol}_{\text{L}}}} \tag{34}$$

Liquid molar holdup (M_{L}):

$$M_{\text{L}} = \frac{\rho_{\text{L}} \text{Long}}{P_{\text{mol}_{\text{L}}}} \left(\pi r^2 - r^2 \arccos\left(\frac{h_{\text{t}}}{r}\right) + h_{\text{t}} \sqrt{r^2 - h_{\text{t}}^2} \right) \tag{35}$$

Vapour molar holdup (M_{V}):

$$M_{\text{V}} = \frac{\rho_{\text{V}} \text{Vol}_{\text{V}}}{P_{\text{mol}_{\text{V}}}} \tag{36}$$

Total molar holdup (M):

$$M = M_{\text{V}} + M_{\text{L}} \tag{37}$$

Liquid flowrate (L):

$$L = C_v x \sqrt{\frac{(P_{\text{t}} - P_{\text{s}}) + g\rho_{\text{L}}(h_{\text{t}} + r)}{\rho_{\text{L}}/\rho_{\text{w}}}} \tag{38}$$

4.3. Optimisation problem

The previously described model equations have been formulated within a simultaneous dynamic optimisation approach. The objective is to minimize the transient time to achieve a new set point temperature in the high-pressure separation tank. Optimisation variables are liquid flowrate in the high-pressure separation tank (L) and residual gas bypass flowrate (G) to the first cryogenic heat exchanger, shown in Fig. 1. There are path constraints that correspond to outlet temperature in residual gas (T_{out}), which is then sent to recompression and re-injected to pipeline. This condition has been handled through inequalities in the optimisation problem. The open loop dynamic optimisation problem has been formulated as

$$\begin{aligned} \min \quad & \int_0^{t_{\text{f}}} (T_{\text{s}} - T_{\text{SP}})^2 \, \text{d}t \\ \text{s.t.} \quad & \{\text{DAE system}\} \\ & 60 \leqslant L \leqslant 130 \ (\text{kmole/min}) \\ & 5 \leqslant G \leqslant 80 \ (\text{kmole/min}) \\ & 303 \leqslant T_{\text{out}} \leqslant 306 \ (\text{K}) \end{aligned} \tag{39}$$

where T_{S} is inlet temperature to the high-pressure separation tank, T_{SP} corresponds to a new set point temperature in this tank. The integral objective function has been handled as an additional differential equation.

The dynamic optimisation model for the shell and tube heat exchangers and the high-pressure separator has been formulated within a Fortran environment. The continuous DAE optimisation problem is transformed into an NLP problem through a full discretisation of state and control variables. The NLP solver is IPOPT [4,2], a barrier method that proceeds by solving parametric NLP subproblems in the barrier parameter (starting from an initial value of 0.01) to a relaxed tolerance.

5. Numerical results

The DAE optimisation problem for the cryogenic heat exchangers and the high-pressure separation tank includes 69 differential and 274 algebraic equations. The resulting large scale NLP, when considering 20 finite elements and two collocation points, has 18,274 discretised variables,

40 of which correspond to optimisation ones (liquid flowrate and residual gas bypass). The problem has required 48 iterations for convergence and it involves the solution of three barrier problems. Optimisation results are shown in Figs. 3–8. The new set point temperature is 211.6 K and it can be achieved in about twelve minutes, from an initial temperature of 212 K (Fig. 3). Profiles for optimisation variables are presented in Figs. 4 and 5; it can be noted that the lower required temperature in the high-pressure separation tank renders a consequent decrease in the residual gas bypass (G), from an initial value of 77.5 kmole/min to 73.2 kmole/min, as now an increased cooling charge is required in the first cryogenic heat exchanger (Fig. 4). It can also be seen that the residual gas outlet temperature from the cryogenic heat exchangers remains within specified bounds along the transient (303 and 306 K). Fig. 5 shows the associated liquid flowrate stream increase in the high-pressure separation tank. Temperature spatial

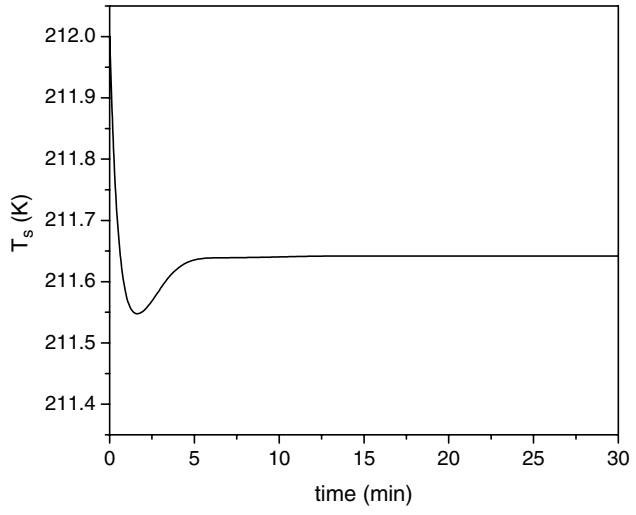

Fig. 3. Optimal temperature profile for high-pressure separation tank (T_s).

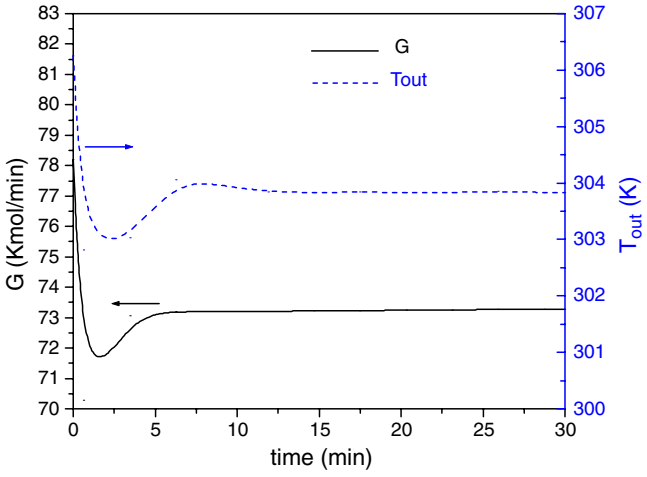

Fig. 4. Optimal profile for residual gas bypass flowrate (G, optimisation variable) and residual gas outlet temperature (T_{out}).

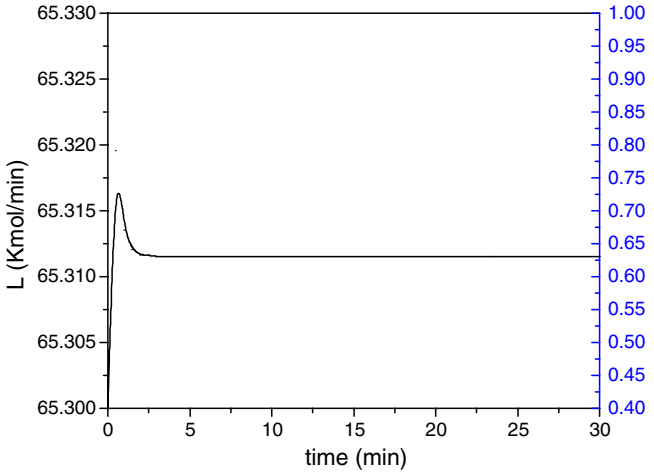

Fig. 5. Optimal profile for liquid stream in high-pressure separation tank (L) and liquid height in the horizontal tank (h_t).

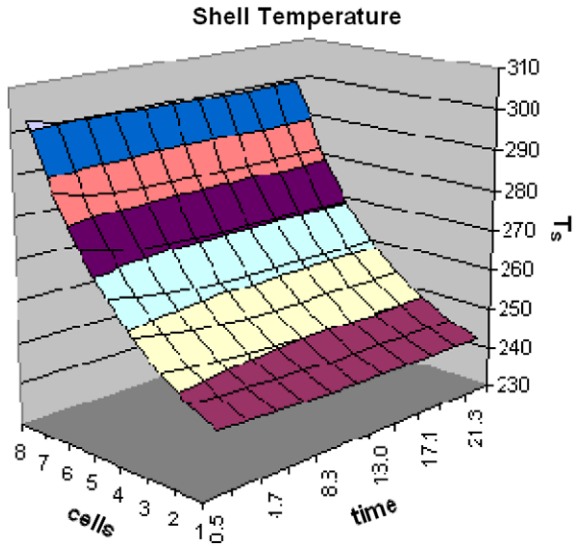

Fig. 6. Temperature profile for first heat exchanger, shell side fluid (T_s).

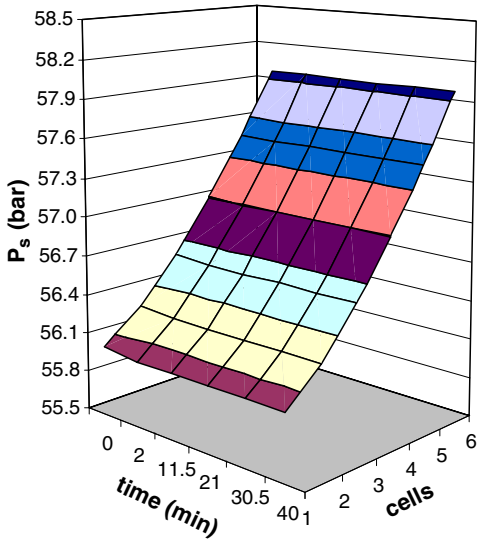

Fig. 7. Optimal pressure profile for shell side fluid in second cryogenic heat exchanger (two-phase flow).

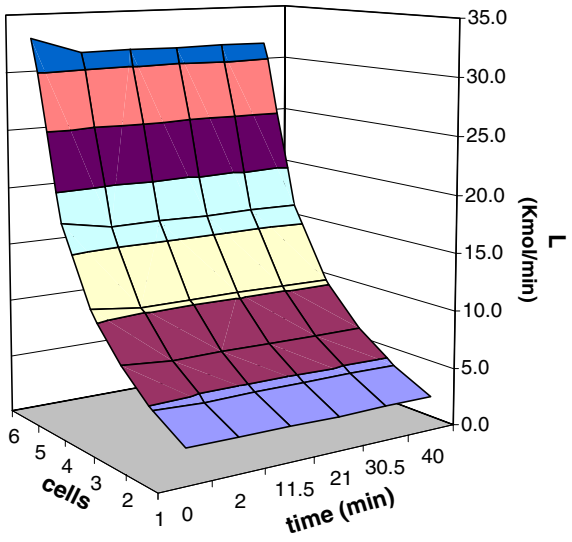

Fig. 8. Optimal liquid flowrate in second cryogenic heat exchanger (two-phase flow).

and temporal profiles in the first cryogenic heat exchanger, shell side fluid, are shown in Fig. 6, where a spatial discretisation of eight cells has been considered. The second heat exchanger behaviour is presented in Figs. 7 and 8, taking into account six cells in the spatially discretised model. Optimal pressure profile in the two-phase flow is shown in Fig. 7, for condensing natural gas. Finally, condensing fluid flowrate is plotted in Fig. 8; it must be noted that liquid fraction in the outlet stream of the cryogenic heat exchanger is in agreement with current plant data, 31 kmole/min, which corresponds to a condensed fraction of 28%.

6. Conclusions

A rigorous dynamic optimisation model has been presented for cryogenic heat exchangers and high-pressure separator from a natural gas processing plant. The dynamic models for the second heat exchanger, where natural gas partial condensation takes place, have required special effort. Optimal profiles have been obtained for control and state variables through the solution of a rigorous dynamic model of process units in the plant. The optimisation DAE problem has been solved with a simultaneous approach that discretises both control and state variables and solves a large scale NLP, with advanced mathematical programming techniques. This strategy has allowed the inclusion of path constraints, as residual gas outlet temperature, in the transient model. The inclusion of rigorous thermodynamic models within a simultaneous approach is also a challenging issue due to the high nonlinearity that is added to the problem by these thermodynamic equations. Model resolution provides optimal temporal and spatial profiles and a great deal of information describing the two-phase flow and fluid separation in the cryogenic sector of a large scale plant.

Appendix A. SRK equation of state

Compressibility factor for a mixture $(z^{\mathrm{V}}, z^{\mathrm{L}})$

$$z = \frac{V}{V-b} - \frac{a\alpha}{R_{\mathrm{T}}(V+b)}$$

where

$$a\alpha = \sum x_j^* z_{1j}^*$$

$$x_j^* = x_j a_j \alpha_j$$

$$z_{1j}^* = \sum_k x_k^* (1 - k_{j,k})$$

$$b = \sum_j b_j$$

$$b_j = 0.08664 \frac{RT_{\mathrm{c}_j}}{P_{\mathrm{c}_j}}$$

$$a_j = \left(\frac{0.42747 R^2 T_{\mathrm{c}_j}^2}{P_{\mathrm{c}_j}} \right)^{0.5}$$

$$\alpha_j = 1 + m_j \left[1 - \left(\frac{T}{T_{\mathrm{c}_j}} \right)^{0.5} \right]$$

$$m_j = 0.48 + 1.574\omega_j - 0.176\omega_j^2$$

Fugacity coefficient for component j in each phase at each stage $(\phi_{i,j}^{\mathrm{V}}, \phi_{i,j}^{\mathrm{L}})$

$$\ln \phi_j = \frac{b_j}{b}(z-1) - \ln(z-B) - \frac{A}{B}\left[\frac{2a_j\alpha_j z_{1j}^*}{a\alpha} - \frac{b_j}{b} \right] \ln\left(1 + \frac{B}{z}\right)$$

Residual enthalpy for each phase $(\Delta H_i, \Delta h_i)$

$$-\frac{\Delta H}{RT} = -1 - \frac{1}{bRT} \ln\left(1 + \frac{B}{z}\right) \sum_j x_j^* z_{1j}^* \left(\frac{1+m_j}{\alpha_j} \right)$$

where

$$A = \frac{a\alpha P}{R^2 T^2}$$

$$B = \frac{bP}{RT}$$

Phase densities at each stage $(\rho^{\mathrm{V}}, \rho^{\mathrm{L}})$

$$\rho = \frac{P}{zRT}$$

References

[1] K.J. Bell, Delware method for shell side design, Petro/Chem Eng. 1 (1960) 26–40.
[2] L.T. Biegler, A. Cervantes, A. Waechter, Advances in simultaneous strategies for dynamic process optimization, Chem. Eng. Sci. 57 (2002) 575–593.
[3] A. Cervantes, L.T. Biegler, Large-scale DAE optimization using simultaneous nonlinear programming formulations, AIChE J. 44 (1998) 1038–1050.

[4] A. Cervantes, A. Waechter, R. Tutuncu, L.T. Biegler, A reduced space interior point strategy for optimization of differential algebraic systems, Comput. Chem. Eng. 24 (2000) 39–51.
[5] D. Correa, J. Marchetti, Dynamic simulation of shell-and-tube heat exchangers, Heat Transfer Eng. 8 (1987) 50–59.
[6] M.S. Diaz, A. Serrani, R. de Beistegui, E. Brignole, An MINLP Strategy for the Debottlenecking problem in an Ethane Extraction Plant, Comput. Chem. Eng. 19s (1995) 175–178.
[7] M.S. Diaz, A. Serrani, A. Bandoni, E. Brignole, Automatic design and optimization of natural gas plants, Ind. Eng. Chem. Res. 36 (1997) 715–724.
[8] M.S. Diaz, S. Tonelli, A. Bandoni, L.T. Biegler, Dynamic optimization for switching between steady states in cryogenic plants, Found. Comput. Aided Process Oper. 4 (2003) 601–604.
[9] C. Lakshmanan, O. Potter, Dynamic simulation of a countercurrent heat exchanger modeling-start-up and frequency response, Int. Commun. Heat Mass Transfer 21 (1994) 421–434.
[10] A. Raghunathan, M.S. Diaz, L.T. Biegler, An MPEC formulation for dynamic optimization of distillation operations, Comput. Chem. Eng. 28 (2004) 2037–2052.
[11] F.E. Romie, Transient response of the counterflow heat exchanger, J. Heat Transfer 106 (1984) 620–626.
[12] G. Soave, Equilibrium constants for a modified Redlich–Kwong equation of state, Chem. Eng. Sci. 27 (1972) 1197–1203.
[13] J. Yin, M. Jensen, Analytic model for transient heat exchanger response, Int. J. Heat Mass Transfer 46 (2003) 3255–3264.
[14] D. Zinemanas, D. Hasson, E. Kehat, Simulation of heat exchangers with change of phase, Comput. Chem. Eng. 8 (1984) 367–375.